High-peak-power vertical-cavity surface-emitting laser quasi-array realized using optimized large-aperture single emitters

2014 Jpn. J. Appl. Phys. 53 070303

(http://iopscience.iop.org/1347-4065/53/7/070303)

Japanese Journal of Applied Physics **53**, 070303 (2014) **RAPID COMMUNICATION**
http://dx.doi.org/10.7567/JJAP.53.070303

High-peak-power vertical-cavity surface-emitting laser quasi-array realized using optimized large-aperture single emitters

Jianwei Zhang, Yongqiang Ning, Xing Zhang*, Jian Zhang, Yugang Zeng, Xianonan Shan, Li Qin, and Lijun Wang

Key Laboratory of Excited State Processes, Changchun Institute of Optics, Fine Mechanics and Physics, The Chinese Academy of Sciences, Changchun, Jilin 130033, P. R. China
E-mail: zjw1985@ciomp.ac.cn

Received April 8, 2014; accepted April 19, 2014; published online June 11, 2014

We report on a high-peak-power vertical-cavity surface-emitting laser (VCSEL) quasi-array emitting at approximately 980 nm. The quasi-array is composed of four tightly packaged single emitters connected in series. The external quantum efficiency of large-aperture VCSEL was improved by optimizing the current distribution, and single emitters with a 62 W peak power were developed as the basic building block of this quasi-array. More than 210 W peak power is demonstrated from a ~2.2 × 2.2 mm^2 quasi-array at a current of 110 A under 30 ns and 5 kHz pulsed operation. This is the first report on a hundreds-of-watts VCSEL module consisting of single emitters. © 2014 The Japan Society of Applied Physics

Vertical-cavity surface-emitting lasers (VCSELs) are very attractive as high-power light sources owing to their advantageous configuration of two-dimensional arrays and their being free of catastrophic optical damage (COD).[1–4] Recently, high-power VCSELs under pulsed operation have attracted much attention owing to their potential applications such as laser fuzing, medical treatment, car-sensing, and laser ranging.[5–10] High-power VCSELs show excellent yield and reliability under short-pulse operation, benefiting from the suppressed self-heating effect within the active region and the absence of COD. Thus, the maximum output powers of 92 W[6] from a single emitter and 123 W[7] from a 16-arrayed emitter have been achieved under short-pulse operation. Moreover, a high-power-density proton-implanted VCSEL array consisting of seven arrayed emitters with a 40 W peak power was reported.[8,9]

Owing to the uniform current distribution at a small current aperture, a VCSEL array can achieve a higher external efficiency,[11] which is the main reason for its higher output power than large-aperture single emitters. However, because of the electrically parallel relationship between all of the element devices, the operating current of a VCSEL array must be very high to achieve a high output power. Actually, a ns-pulse current source with hundreds of amperes is technically difficult to realize. Additionally, the electrical and thermal crosstalk[12,13] between all the elements of an array would become very serious at a high current. Thus, large-aperture single emitters were developed in this work. It was shown that the performance of VCSEL single emitters could be improved by optimizing their current distribution. Moreover, an external quantum efficiency of 0.62 W/A was gained for a large-aperture single emitter. A 2.2 × 2.2 mm^2 VCSEL quasi-array consisting of four tightly arranged single emitters was proposed, and a high peak power of 210 W under 30-ns-pulse operation was achieved at an operating current of 110 A. The corresponding external quantum efficiency was 1.91 W/A.

A schematic view of our 980 nm VCSEL structure is shown in Fig. 1. The n-distributed Bragg reflector (DBR) layers, the active region, and the p-DBR layers were sequentially grown on the n-GaAs substrate by metal–organic chemical vapor deposition (MOCVD). The active region was composed of three 8-nm-thick $In_{0.2}Ga_{0.8}As$ quantum wells for an emission wavelength of about 980 nm. For selective oxidation, a 30-nm-thick $Al_{0.98}Ga_{0.02}As$ layer was partially used instead of a high-Al-content layer in the p-side DBR, near the active region.

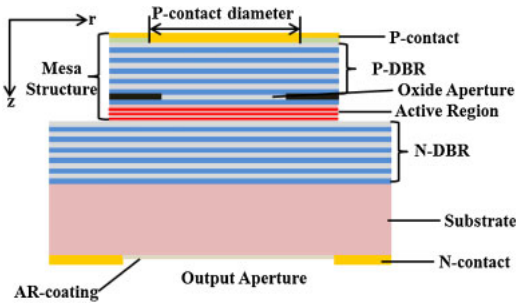

Fig. 1. (Color online) Schematic diagram of the 980 nm VCSEL structure.

The mesa structure of VCSEL was formed by ICP etching. After mesa etching, current apertures were formed by wet oxidization, under the following oxidization conditions: 420 °C under 30 sccm N_2 gas bubbled through 90 °C deionized water. A SiO_2 insulating layer was deposited on the mesa using PECVD and then etched away partially to form an electrode window. Au-based electrodes were sputtered on p-sides of the devices. Finally, an antireflection coating layer and an Au-based film were evaporated on the GaAs substrate to form an emission window and an n-electrode, respectively. The VCSEL devices were cleaved and mounted on a TO package to ensure its rapid response to the ns-pulse current source. Packaged VCSEL single emitters and module were operated using a short-pulsed current with a 30-ns-pulse width and a 5 kHz repetition rate at room temperature. The operating conditions of VCSEL were consistent with its applications in laser fuzing and laser ranging.

To realize a uniform current distribution, VCSELs with varying p-contact and oxide aperture diameters were proposed. We have developed a three-dimensional finite-element model to calculate the current-density distribution in the active region of bottom-emitting VCSELs. Under the stationary-state condition, the electrical potential U in VCSELs is determined by Laplace's equation and the corresponding boundary conditions:[14,15]

$$\nabla \cdot (\sigma \cdot \nabla \cdot U) = 0, \tag{1}$$

$$U(r, z = 0) = U_0, \tag{2}$$

$$U(r, z = d_{\mathrm{VCSEL}}) = 0, \tag{3}$$

$$\frac{dU}{dr} = 0 \, (r = R_{\text{p-contact}},\ 0 < z < d_{\text{p-contact}}), \tag{4}$$

where U_0 is the potential drop across the whole VCSEL and d_{VCSEL} is the thickness of the VCSEL. $R_{\text{p-contact}}$ and $d_{\text{p-contact}}$ are the radius and thickness of the p-contact, respectively. The conductivity σ is defined by a vector matrix:

$$\sigma = \begin{pmatrix} \sigma_r & 0 \\ 0 & \sigma_z \end{pmatrix}. \tag{5}$$

The anisotropic conductivity of multilayer structures is determined using the following expressions:

$$\sigma_r = \frac{d_1\sigma_1 + d_2\sigma_2}{d_1 + d_2}, \quad \sigma_z = \frac{d_1 + d_2}{d_1/\sigma_1 + d_2/\sigma_2}, \tag{6}$$

where σ_1 (σ_2) and d_1 (d_2) are, respectively, the conductivity and thickness of layer 1 (layer 2). By solving

$$J_z = \sigma_z \cdot \nabla U, \tag{7}$$

the current density J_z injected into an active region in the longitudinal direction is calculated. With an constant injection current of 3 A, the current densities J_z were compared among VCSELs with different configurations, as shown in Fig. 2.

The minimum current aperture diameter of the simulated VCSELs is 200 μm, which corresponds to the reported critical aperture size in Ref. 5. As shown in Fig. 2, the effect of the p-contact diameter on the current distribution is dependent on the oxide aperture diameter. All the three VCSEL structures show the current crowding effect at the edge of the active region as the p-contact diameter approaches the oxide aperture diameter. However, the crowding effect becomes more serious for VCSELs with a larger oxide aperture.

For an oxide aperture diameter of 200 μm, the p-contact diameter has a significant impact on the current distribution, as shown in Fig. 2(a). The high current density appears at the center part of the active region for a 100 μm p-contact. By increasing the diameter of the p-contact, a uniform current density distribution within the active region is achieved. However, the current crowding effect at the edge is observed when the diameter of the p-contact exceeds 160 μm.

The effect of the p-contact diameter on the current distribution is less significant for oxide aperture diameters of 300 and 400 μm, as shown in Figs. 2(b) and 2(c), respectively. Current crowding at the edge of the active region also occurs for all p-contact diameters. To suppress the excitation of high-order modes, the current density at the edge should be kept lower than that at the center. For VCSEL with an oxide aperture diameter of 300 μm, a p-contact with a 240 μm diameter is considered suitable [dotted line in Fig. 2(b)]. For an oxide aperture diameter of 400 μm, the current distribution does not differ markedly when the p-contact is larger than 340 μm, and current crowding at the edge of the active region is very serious, as shown in Fig. 2(c). Also the current distribution along the active region is not sufficiently uniform for a 300-μm-diameter p-contact. Thus, a 320-μm-diameter p-contact is chosen for a 400-μm-diameter oxide aperture [dashed line in Fig. 2(c)].

From the above discussions, VCSEL structures with oxide apertures of 200, 300, and 400 μm were fabricated, and the optimized p-contact diameters were 160, 240, and 320 μm, respectively. The near-field patterns of these three VCSELs are shown in Fig. 3. The VCSEL with a 200 μm oxide aperture shows a uniform emission profile in Fig. 3(a), owing

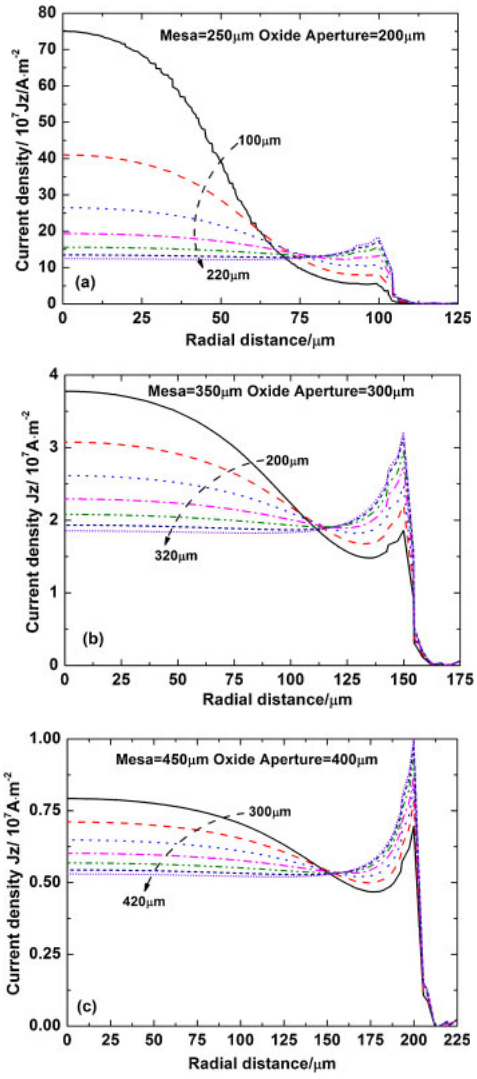

Fig. 2. (Color online) Current density profiles along the radius of active region for the oxide aperture diameters of (a) 200, (b) 300, and (c) 400 μm, with varying p-contact diameter. The mesa diameter is 50 μm larger than the oxide aperture diameter and the p-contact diameter varies in 20 μm increments.

to its uniform current distribution. A small amount of nonuniform emission with a low intensity is observed in the near-field profile of VCSEL with a 300-μm-diameter oxide aperture, as shown in Fig. 3(b). The spatial multimode emission caused by the current density peak is thought to be the main reason for this.[16] For the device with a 400-μm-diameter oxide aperture, serious current crowding at the edge leads to a preferred lasing at the edge of the active region, and this phenomenon suppresses the carrier recombination at the center part of active region. Thus, an annular near field profile is observed in Fig. 3(c).

The light vs current (L–I) characteristics of these three VCSELs were measured under QCW and ns-pulse operation, and are shown in Fig. 4. Thermal rollovers are observed in Fig. 4(a), which are due to the self-heating effect in the active region of VCSEL under QCW operation. VCSEL with a 200-μm-diameter oxide aperture shows a thermal rollover firstly, which is caused by a serious self-heating due to its high current density in the active region. VCSEL with 300-μm-diameter oxide aperture shows a maximum output power of these three

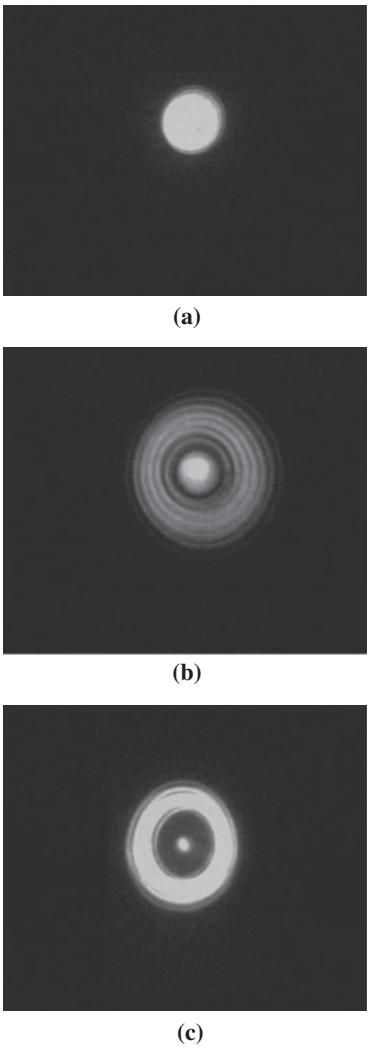

Fig. 3. Near-field pattern of three VCSEL samples with (a) 200-, (b) 300-, (c) 400-μm diameter oxide apertures, operated by 3 A current under 100 μs quasi-CW (QCW). The corresponding p-contacts were 160, 240, and 320 μm.

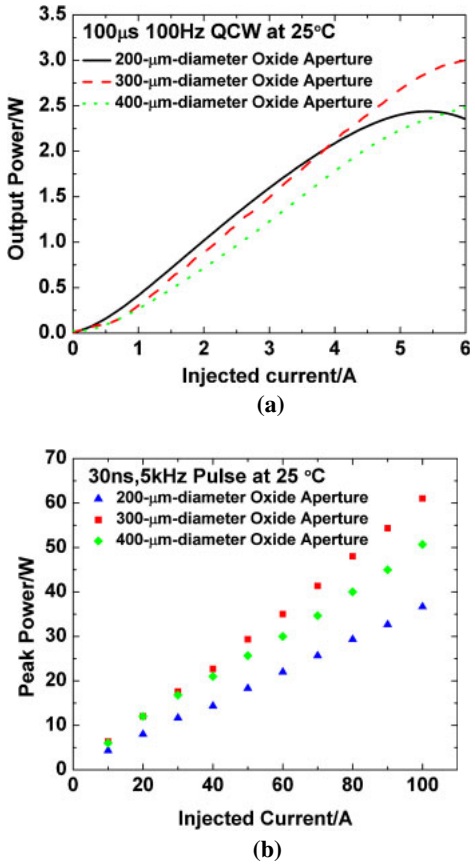

Fig. 4. (Color online) *L–I* characteristics of three samples under (a) QCW and (b) ns-pulse operation.

samples, and the output power of 3 W is reached. For VCSEL with a maximum oxide-aperture diameter of 400 μm, the lasing region is mainly concentrated at the edge of active region. Thus, the luminescence efficiency of carrier recombination in the active region is very low. And the corresponding external efficiency is rather low, as shown in Fig. 4(a).

The output power characteristics under ns-pulse operation for the three single emitters are shown in Fig. 4(b). Thermal rollovers are not observed in all the samples, since the heat generation of VCSELs is suppressed owing to the relatively short-pulsed operations. VCSEL with a current aperture of 200 μm has the lowest external efficiency, and a serious carrier leakage under a very high current density is considered to be the main reason for this. Carrier leakage within the active region may occur when numerous carriers are injected into quantum wells (QWs) under high-level short-pulsed operation. The leaked carriers cannot recombine to emit light, and this decreases the internal efficiency of QWs. Also the external efficiency of VCSEL is decreased. For VCSEL with a 200-μm-diameter oxide aperture, the current density within the active region is more than ten times that of the other two apertures at the same injection current, as shown in Fig. 2. Thus, the carrier leakage in this VCSEL is more serious than in the other VCSELs. However, power saturation is not observed as the 200-μm-diameter oxide aperture is sufficiently large to support the high-level short-pulsed operation. This is homologous to the critical aperture size reported by Otake et al.[5)]

For VCSEL with the oxide aperture diameter of 400 μm, its lower external efficiency than VCSEL with the 300-μm-diameter oxide aperture is observed. The nonuniform current distribution within the 400-μm-diameter oxide aperture is the main reason for this, as shown in Fig. 2(c). By setting the diameter of the oxide aperture and p-contact to 300 and 240 μm, an external efficiency of 0.62 W/A was gained, which has reached the reported result of five-quantum well VCSEL devices in Ref. 5. Moreover, the maximum power of 62 W is achieved, which was higher than the record power of proton-implanted single emitters and arrays.[8)]

As the VCSEL array shows disadvantages such as high operation current, and electrical and thermal crosstalk, a VCSEL quasi-array consisting of four single emitters is developed in this communication. The large-aperture single emitter with a 300-μm-diameter oxide aperture and a 240-μm-diameter p-contact was adopted as the basic building block owing to its good performance. The configuration of this quasi-array has been optimized to achieve the shortest gold wire connection; thus, the short-pulse response of VCSEL was ensured. A schematic diagram of the VCSEL quasi-array is shown in Fig. 5. The side length of this square module is about 2.2 mm. VCSEL-chip units are soldered onto

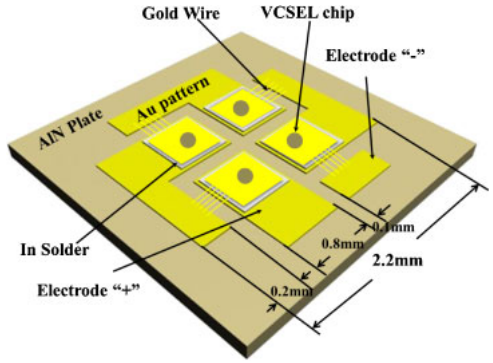

Fig. 5. (Color online) Schematic diagram of the VCSEL quasi-array consisting of four single emitters connected in series.

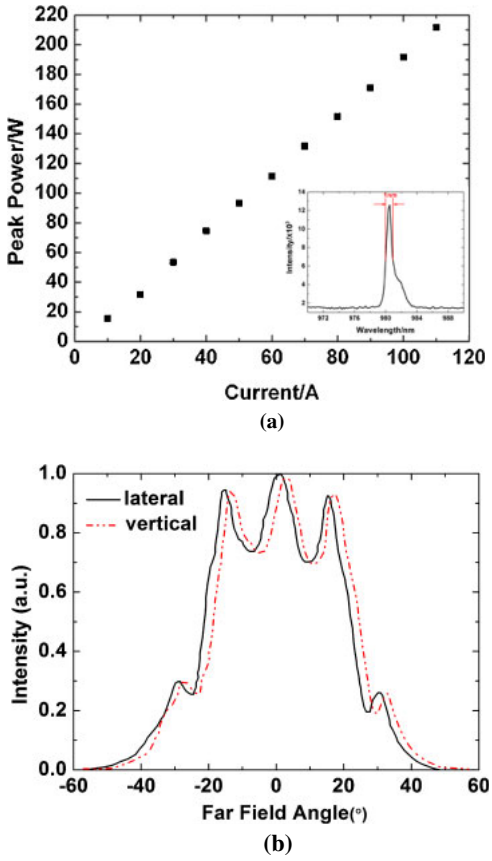

Fig. 6. (Color online) (a) *L–I* characteristics and (b) far-field pattern at 110 A of VCSEL quasi-array under ns-pulse operation. The wavelength spectrum at 110 A is inserted in (a).

a high-thermal-conductivity AlN plate and then connected in series. Then the whole module is packaged onto a TO-39 holder.

The pulsed *L–I* characteristics and wavelength spectrum at 110 A are shown in Fig. 6(a). The pulse width and repetition rate are 30 ns and 5 kHz, respectively. The VCSEL module exhibits a peak output power of 210 W at a pulsed current of 110 A in Fig. 6(a), limited by the power supply. The output power of the VCSEL module is smaller than the sum of the output power of four single emitters. And that may be related to the current loss caused by the inductance and capacitance in the circuit. However, to the best of our knowledge, this is the highest value reported for the VCSEL module consisting of single emitters. The insert in the figure shows the wavelength spectrum at 110 A. The central wavelength is 980.5 nm and the full-width at half-maximum (FWHM) is 1 nm.

The far-field pattern of the quasi-array is shown in Fig. 6(b). Side lobes are observed from the intensity distribution, originating from the large number of high-order modes of the single emitter and from the modal interference.[16] The divergence angle (FWHM) is more than 40° under an injected current of 110 A, which is rather unfavorable for its applications. However, the intensity distribution and divergence angle of VCSELs can be easily tailored by the collimating microlenses and field lenses.[17] In fact, the beam shaping of high-peak-power VCSELs is necessary for many applications such as laser ranging and laser fuzing. Related investigations will be carried out in our following research.

In summary, VCSELs with different diameters of the p-contact and oxide aperture was fabricated to optimize its performance under a high injected current. A peak output power of 62 W is obtained from a single emitter with a 300-μm-diameter current aperture. A VCSEL module consisting of four such single emitters was developed, and a maximum peak output power of 210 W was achieved, which is the highest value reported for VCSEL modules consisting of single emitters. We believed that the small area and high output power of our module promise wide application prospects.

Acknowledgments This work is supported by the National Natural Science Foundation of China under Grant Nos. 61204056, 61234004, and 61376070, the Foundation of Jilin Province under Grant No. 20140520113JH, and the Foundation of Jiangsu Province under Grant No. BK2012188.

1) K. Iga, IEEE J. Sel. Top. Quantum Electron. **6**, 1201 (2000).
2) L. A. D'Asaro, J. F. Seurin, and J. D. Wynn, Photonics Spectra **39**, 64 (2005).
3) K. Ding and C. Z. Ning, Light Sci. Appl. **1**, e20 (2012).
4) J. F. Seurin, C. L. Ghosh, V. Khalfin, A. Miglo, G. Y. Xu, J. D. Wynn, P. Pradhan, and L. A. D'Asaro, Proc. SPIE **6876**, 68760D (2008).
5) N. Otake, K. Abe, H. Yamada, H. Wado, and Y. Takeuchi, Appl. Phys. Express **2**, 052102 (2009).
6) L. Zhang, Y. Ning, Y. Zeng, L. Qin, Y. Liu, X. Zhang, D. Liu, H. Xu, J. Zhang, and L. Wang, Appl. Phys. Express **4**, 052102 (2011).
7) D. Liu, Y. Ning, Y. Zeng, L. Qin, Y. Liu, X. Zhang, L. Zhang, J. Zhang, C. Tong, and L. Wang, Appl. Phys. Express **4**, 052104 (2011).
8) H. Naito, M. Miyamoto, Y. Aoki, A. Higuchi, K. Torii, T. Nagakura, T. Morita, J. Maeda, H. Miyajima, and H. Yoshida, Appl. Phys. Express **5**, 082104 (2012).
9) H. Naito, M. Miyamoto, Y. Aoki, A. Higuchi, K. Torii, T. Nagakura, T. Morita, J. Maeda, H. Miyajima, and H. Yoshida, Proc. SPIE **8639**, 86390N (2013).
10) K. Sugioka and Y. Cheng, Light Sci. Appl. **3**, e149 (2014).
11) J. F. Seurin, C. L. Ghosh, V. Khalfin, A. Miglo, G. Xu, J. D. Wynn, P. Pradhan, and L. A. D'Asaro, Proc. SPIE **6908**, 690808 (2008).
12) K. J. Greenberg, J. A. Summers, and J. A. Hudgings, IEEE Photonics Technol. Lett. **22**, 655 (2010).
13) J. Wang, I. Savidis, and E. G. Friedman, Microelectron. J. **42**, 820 (2011).
14) X. Zhang, Y. Ning, Y. Zeng, J. Zhang, X. Fu, L. Qin, Y. Liu, C. Tong, and L. Wang, IEEE J. Quantum Electron. **48**, 42 (2012).
15) C. Angelos, S. Hinckley, R. Michalzik, and V. Voignier, Proc. SPIE **5277**, 261 (2004).
16) S. Gronenborn, J. Pollmann-Retsch, P. Pekarski, M. Miller, M. Strösser, J. Kolb, H. Mönch, and P. Loosen, Appl. Phys. B **105**, 783 (2011).
17) H. Moench, S. Gronenborn, M. Miller, and P. Loosen, Proc. SPIE **7952**, 795207 (2011).